Design and Construction of an Experimental Wave Energy Device Emulator Test Rig

J. Duquette[1], D. O'Sullivan[1], S. Ceballos[2] and R. Alcorn[1]

[1] Hydraulics and Maritime Research Centre,
University College Cork,
Youngline Industrial Estate, Pouladuff Road, Cork, Ireland

[2] Robotiker-Tecnalia,
Energy Unit, Parque tecnologico de Zamudio,
Edif. 202, 48170, Zamudio, Spain

Abstract

An experimental test rig has been constructed which is capable of recreating within a laboratory setting the dynamic response exhibited by a prime mover onto a motor – generator assembly. The prime mover can simulate from real or modeled time series data any varying source such as a wind turbine, a hydraulic motor or a wave energy air turbine.

The initial application around which the test rig has been designed is a wave energy converter. In this regard, the case study considered in this paper is the emulation of a floating Oscillating Water Column – Wells turbine device operating under a number of sea states. Particular attention has been given to the control algorithm of such a converter and to the effect on device performance including the flywheel storage. Simulations were conducted in Matlab/Simulink and results demonstrate by means of peak to average power ratios that significant improvements in the system's performance were achieved for any given sea state with the addition of a flywheel energy storage device. In particular, the ratios for power exported to the grid were seen to improve by up to a factor of 4.5.

Keywords: Flywheel energy storage, Induction generator, Oscillating water column, Wave energy device, Wells turbine

Nomenclature

J	=	inertia
m	=	mass
r	=	radius
ω	=	angular velocity
P	=	power
V	=	voltage
s	=	slip
n	=	turns ratio
H	=	wave height
t	=	time
p	=	pressure
Q	=	airflow
λ	=	scale factor
η	=	efficiency
Phi	=	dimensionless flow coefficient
v	=	flow velocity
U	=	tip velocity
A	=	cross-sectional area
D	=	diameter
N	=	rotational speed
M	=	torque
ρ	=	density
h	=	thickness
pi	=	trigonometric constant

Subscripts

fw	=	flywheel
dt	=	drivetrain
elec	=	electrical
mech	=	mechanical
pneu	=	pneumatic
a	=	air
t	=	turbine
D	=	duct
h	=	hub
avg	=	average
min	=	minimum
max	=	maximum

1 Introduction

Ocean energy has long been considered an abundant renewable resource with a tremendous potential for electrical power production worldwide. The earliest development efforts in ocean energy technology worth noting took place in the mid 1970s when public interest in alternative energy research flared worldwide mostly as a result of the crippling effects of the oil embargo on energy addicted nations. Since then, a multitude of energy conversion devices have been designed and tested which are capable of harnessing the ocean's energy both onshore and offshore and converting it to useable electrical power [1,9]. Until recent years, research in ocean energy was slow-going and even the

most advanced devices were either too expensive to build or inherent flaws persisted meaning that serious technological barriers needed to be overcome before commercial viability could even be considered [2]. Only recently have these barriers begun to lower at an increasingly rapid rate. This is primarily due to the remarkable advances made in power electronics technology, mostly pioneered by the flourishing wind energy industry. Low cost variable speed compact drives have been made available on the market which allow for very high efficiencies to be reached and virtually eliminate the need for many otherwise required components on older turbine-generator systems such as a gearbox.

Many natural phenomena such as coastal topography, climate, underwater currents and the rising and falling tides significantly influence local sea conditions and ultimately define the means by which power may be extracted in any given geographical area. Ireland boasts one of the most energetic wave climates in the world and due to this there has been considerable interest at the national level to further invest in wave energy technologies [3]. A recent research initiative was undertaken at the Hydraulics and Maritime Research Centre (HMRC) in Cork Ireland in which an experimental test rig was designed and constructed. The test rig is capable of recreating within a laboratory setting the dynamic response exhibited by a prime mover onto a motor – generator set and simultaneously measuring the outgoing power quality. The prime mover can simulate from real or modelled time series data any varying source such as a wind turbine, a hydraulic motor or a wave energy air turbine. As HMRC is dedicated foremost to ocean energy research, the primary application around which the test rig has been designed is a wave energy converter. The test rig is an extremely flexible tool in that it enables the optimization of a wide range of energy converter systems under various conditions. It is also a very useful tool in that the functionality of the wave energy converter under study can be almost entirely predicted at nearly all levels from wave to wire before any lengthy and expensive on-site sea trials are to be performed.

The test rig is primarily constructed from two, three phase, 20 kW induction machines which are coupled together and separately controlled by variable speed drives. The first machine acts as the prime mover and the second machine acts as a multi-configurable generator. The electrical power thereafter returns to the AC mains network via impedance networks which are used to emulate typical power lines and transformers at specified distances from a strong grid connection point. Current and voltage sensors, located in between the impedance networks, transmit readings to a Programmable Automation Controller (PAC) which stores the data for subsequent power quality studies. Additionally, a number of safety features have been incorporated into the test rig and the option of utilizing a flywheel energy storage device has been included in order to reduce fluctuations in the outgoing electrical power for situations where such a requirement exists.

In the following sections, the physical specifications of the test rig will be outlined and a case study will be presented utilizing data from a floating Oscillating Water Column (OWC) – Wells turbine device operating under a range of sea states.

2 Test Rig Specifications

The main constituents that make up the test rig are the drive train assembly (prime mover, generator, gearbox and flywheel energy storage system), control system, data acquisition system, grid emulator and protection equipment. The block diagram in Fig. 1 illustrates the system as a whole.

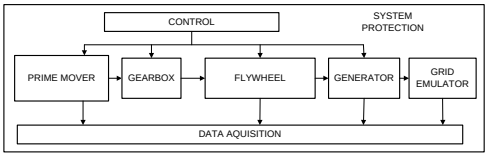

Figure 1: Test rig system configuration

2.1 Drive Train Assembly

The drive train assembly is made up of all the moving parts in the test rig. The prime mover is a 20 kW, 3 phase, 4 pole induction machine. The generator is almost identical with the exception that the rotor is equipped with slip rings. Access to the rotor windings allows the generator to be wired as a squirrel cage, doubly fed or variable resistance generator depending on user preference. A separate synchronous generator configuration can also be added if desired. The other drive train constituents are a 4 speed gearbox (with ratios of 1, 1.576, 2.538, 4 and neutral) and a flywheel device. The stainless steel flywheel has a diameter of 0.6 m, a thickness of 80 mm and weighs 180 kg. Additionally, a torque transducer (located in between the motor and the generator) has been fitted. The drive train assembly is shown to scale in Fig. 2.

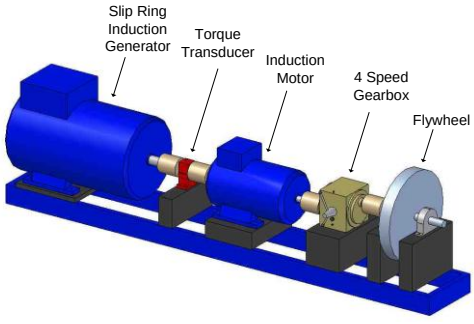

Figure 2: Test rig drive train components

2.2 Data Acquisition & Control

To get a better idea as to how the whole system is laid out, Fig. 3 shows the test rig circuit diagram. All of the data acquired from the test rig as well as the control algorithms are processed through a central

Programmable Automation Controller (PAC). The PAC is equipped with digital input/output modules, analog input modules, a number of RS485/RS232 serial ports, a USB port and an Ethernet port. The RS485 serial communication ports are used to send either a speed or torque reference signal to both variable speed drives assigned to control the motor and generator independently.

a schematic diagram of each generator type are shown in Table 1. The option for multiple generator configurations adds versatility to the system in that the test rig can provide experimental results for a wider array of scenarios.

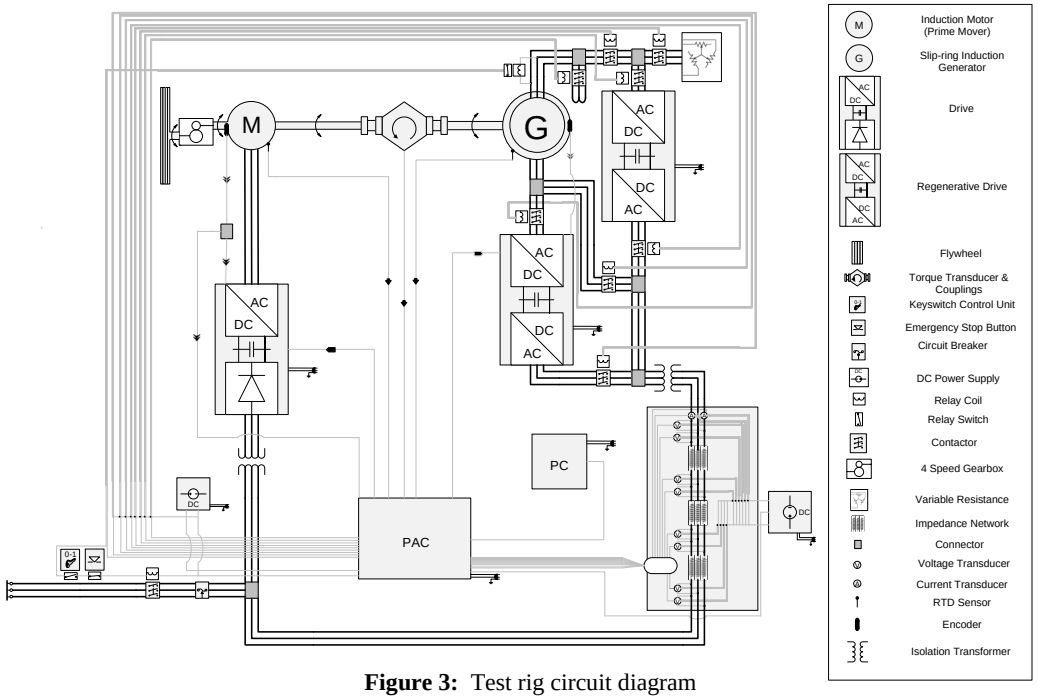

Figure 3: Test rig circuit diagram

Communication between the PAC and the drives is achieved via the 2 wire Modbus RTU protocol. The motor side drive is a 22 kW combined rectifier – inverter unit capable of operating in closed loop vector mode while referencing exact values of speed and encoder position for all internal error calculations. The incremental encoder is rated at 1024 pulses per revolution and is connected to both the drive and the PAC. The extra connection to the PAC allows the implementation of alternative control strategies. The generator is controlled by a 20 kW regenerative drive composed of two back to back converters and allows for bi-directional power flow to and from the AC supply. Additionally it contains a built-in harmonics filter to interface with the grid. A close-up of the area surrounding the generator in Fig. 3 is shown in Fig. 4. The schematic diagram reveals a number of contactors labelled from C1 to C8. The triple pole single throw (TPST) contactors are AC-3 rated at 25 kW. They are activated by 24 volt DC coils from the PAC's digital output module and are used to switch the system to one of three allowable generator configurations. The configurations allow either squirrel cage, doubly-fed or variable resistance induction generator operation depending on each contactor's switch position. A synchronous generator configuration may also be implemented, though it is not present in the current design, by symmetrically distributing DC current over the rotor windings. The contactor positions along with

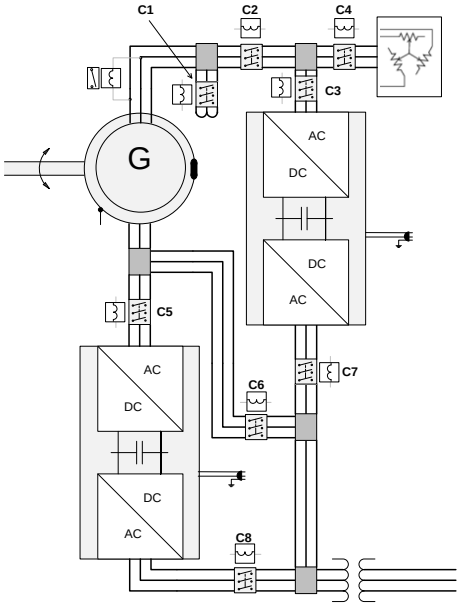

Figure 4: Multi-configurable generator schematic

Table 1: Contactor switch position relative to generator configuration

	Squirrel cage (Fixed speed)	Squirrel cage (Variable speed)	Doubly-fed	Variable resistance
C1	closed	closed	open	open
C2	open	open	closed	closed
C3	open	open	closed	open
C4	open	open	open	closed
C5	open	closed	open	open
C6	closed	open	closed	closed
C7	open	open	closed	open
C8	open	closed	open	open
	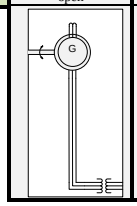	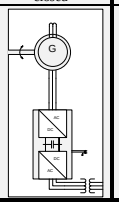	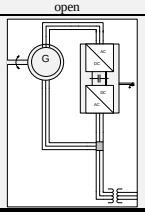	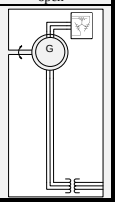

Furthermore, while the test rig is in operation, torque, speed, temperature, voltage and current data are continuously acquired and displayed on the PC user interface for monitoring purposes. The data acquisition and control system is fully programmed using National Instruments' LabView software.

2.3 Grid Emulator

The grid emulator serves to re-create grid-like conditions at various connection points between the device and the AC network. This is accomplished by introducing a number of impedance networks with impedance values corresponding to a specified cable distance. The setup is analogous to a generator situated far from a strong grid connection point with various connection points in between. The grid emulator arrangement is portrayed in the lower right-hand side of Fig. 3. It is solely composed of two current sensors and eight voltage sensors separated by impedance networks. The current sensors have a nominal RMS current rating of 50 A and the voltage sensors are rated at 500 V RMS. When supplied by a DC voltage of +/- 15 V, the sensors deliver a secondary nominal RMS current to the PAC's 16 bit analog input module. In order to accurately study the power quality, a harmonic analysis must be conducted on the recorded current and voltage data. In harmonic studies, it is desirable to consider frequency components up to the fiftieth harmonic of the fundamental. For the purpose of the test rig, connected to a 50 Hz grid, this corresponds to a frequency of 50 X 50 Hz = 2.5 kHz. However, in order to accurately compensate up to the fiftieth harmonic, a sample rate greater than 5 kHz should be used. This is in accordance with the Nyquist Shannon sampling theorem which states that the frequency of the samples must be slightly higher than twice the frequency of the original wave [4]. The impedance networks, illustrated in Fig. 3 as squares containing three coils, were sized with the proper impedance in order to simulate a cable distance of approximately 25 km [5]. Each one is made up of inductive coils in series with each phase and capacitors in parallel with each phase, as shown in Fig. 5.

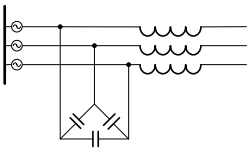

Figure 5: Schematic Diagram of impedance network assembly showing inductive coils in series with each phase and capacitors in parallel with each phase.

2.4 Flywheel

A flywheel power control system makes use of inertial energy storage within a spinning mass. As the rotational speed of the mass increases, energy is absorbed and as the rotational speed decreases, energy is released. This behaviour can be described by Equations (1) and (2) where J, m, r and ω are inertia, mass, radius and angular velocity respectively.

$$\mathrm{J} = \frac{1}{2}\mathrm{mr}^2 \tag{1}$$

$$\mathrm{E} = \frac{1}{2}J\omega^2 \tag{2}$$

Since the radius term in Equation (1) is squared, it can be said that the greater the radius of the flywheel, the smaller the mass required to hold the same inertia. Equally, due to the squared angular velocity term in Equation (2), the greater the speed of the flywheel, the smaller the change in speed needed to store the same amount of energy [6]. The power absorbed or released by the flywheel, P_{fw}, in a motor-generator assembly can be written as shown in Equation (3) when not taking into account efficiency losses.

$$\mathrm{P_{fw}} = (P_{elec} - P_{mech}) - P_{dt} \tag{3}$$

where P_{elec} is the electrical power produced by the generator, P_{mech} is the mechanical power exerted by the motor and P_{dt} is the power absorbed or released due to the drive train inertia (not counting the flywheel). If P_{elec} and P_{mech} are different, a torque imbalance results in the system causing the speed of the flywheel to change. This being said, it is clear that controlling speed can be an effective means of controlling the power absorbed or released by the flywheel, hence energy could be stored or retrieved on demand. P_{fw} can also be calculated by deriving Equation (2) with respect to time, shown in Equation (4).

$$P_{fw} = \frac{dE}{dt} = \frac{dE}{d\omega}\left(\frac{d\omega}{dt}\right) = J\omega\left(\frac{d\omega}{dt}\right) \tag{4}$$

2.5 Protection Equipment

A number of safety features were added to the test rig for the purpose of protecting the equipment and the people using the equipment if anything were to go wrong. The safety components are shown in Fig. 3 and comprise a main shut-off contactor, a 2 position keyswitch, an emergency stop button, an overvoltage relay which connects to the rotor windings of the generator and a secondary contactor circuit which is connected to the contactor's auxiliary contacts. The main system shut-off contactor is normally open and only closes if all the other safety features are operating properly. The two position key switch is normally open, therefore only when the key is turned on will the main system shut-off contactor close. Similarly the emergency stop button is normally closed and when pressed, opens the circuit de-energizing the coil, thus disabling the main contactor. The overvoltage relay is located within the same circuit and is normally closed. If the voltage in the leads stemming from the rotor of the generator is too high, approximately 500 volts or higher, the switch opens and the main system shut-off contactor is opened as a result. The need for this safety feature arises due to the fact that a slip ring induction generator behaves very much like a moving transformer. Unlike a standard transformer where the ratio shown in Equation (5) applies, the slip ring induction generator has an added slip factor. Equation (6) describes how voltage, V, slip, s, and the turns ratio, n, are related from the rotor to the stator.

$$\frac{V_2}{V_1} = \frac{n_2}{n_1} \tag{5}$$

$$\frac{V_{rotor}}{V_{stator}} = \frac{n_{rotor}}{n_{stator}} \times s \tag{6}$$

If the machine is designed to yield a voltage ratio of nearly 1 at nominal conditions, the turns ratio would be set in accordance with the slip at that working point. For example if the nominal slip were 0.1, then the turns ratio would be 10. The problem arises at startup when the slip is high and very high voltages are generated in the rotor circuit. One way to get around this is to wait until the generator has run up to speed and the slip is low, before connecting the stator to the grid. The overvoltage relay protects the system in case the standard starting procedure is not followed or if any other problem should occur. Another important safety feature is the secondary circuit connected to the auxiliary contacts of the contactors. The auxiliary contacts are connected to a +/- 10 V power source as well as to the PAC's analog input module. Pull-up resistors are located in each contactor circuit so that when the auxiliary contact is open, +10 V will be read in the analog module and when the contact is closed, 0 V will be read. The circuit serves as a backup system sending a physical reading of the contactor position to the PAC. Since the contactor arrangement determines the generator configuration, it is of utmost importance that no error be present else major damage to the drives may occur. LEDs are also placed in-line with the resistors as a visual reference to the contactor's position. The remaining safety components also illustrated in Fig. 3 are the main circuit breaker and isolation transformers. The main circuit breaker is of the thermal magnetic type utilized in 3 pole systems with tripping characteristic C and is rated at 50 A and 415 VAC. A 3 phase 400 V to 400 V isolation transformer is located at the system inlet and outlet and provides galvanic insulation from the grid. The transformers are rated at 25 kVA and can handle currents up to 63 A.

3 Oscillating Water Column (OWC) – Wells Turbine Case Study

The case study considered in this paper is the emulation of a floating OWC – Wells turbine device operating under a number of sea states. The block diagram for the system is shown in Fig. 6 and differs from the diagram in Fig. 1 in that the prime mover has been replaced with a Wells turbine emulator composed of a virtual and a physical component.

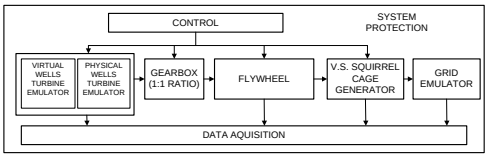

Figure 6: System configuration for OWC – Wells turbine case study

Also, the gearbox has been set to a 1:1 ratio and the variable speed squirrel cage generator configuration was chosen.

3.1 The OWC – Wells Turbine Energy Converter

The OWC effectively converts energy by transforming hydrodynamic wave action into reciprocating airflow. The design consists of a hollow tube or capture chamber, partially submerged, which is open to the sea below the water line. As waves roll in from the ocean, the water column rises and falls and as a result causes the air pressure at the top of the column to act accordingly. A reciprocating air flow is then created through a power take-off device (usually an air turbine) which can be coupled to a generator to produce useful power. The capture chamber is designed to match the power take-off device (and vice-versa) in order to maximise conversion efficiency and is constructed to be resonant at the predominant wave frequencies found at the station site. Due to the bidirectional nature of the air flow, a special turbine design must be utilised in order to allow for self-rectification. One of the most commonly used self-rectifying turbines is the Wells turbine. The Wells turbine is simple, reliable and durable. The rotor design encompasses a central hub with symmetrical airfoil blades mounted around its axis. The airfoil blades act to provide a lift force and a drag force due to the pressure differential across the blades. The main

advantage of using this turbine is that it keeps its sense of rotation in spite of the changing direction of the air stream, which is driven by the rising and falling water level in the column. An illustration of a shoreline OWC – Wells turbine energy converter is shown in Fig. 7.

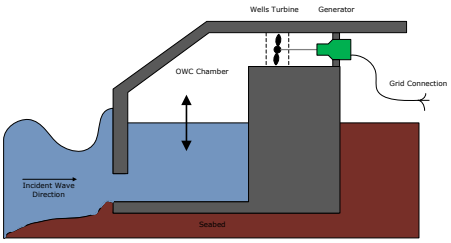

Figure 7: Schematic diagram of a shoreline OWC – Wells turbine energy converter

3.2 The Physical Wells Turbine Emulator

The physical turbine emulator is made up of a number of components and essentially physically behaves as a real turbine would. The components in the test rig which correspond to the turbine emulator are the PAC, the drive and the motor as well as a portion of the flywheel mass which will emulate the turbine inertia.

3.3 The Virtual Wells Turbine Emulator

The virtual turbine emulator is the non physical part of the turbine emulator which is programmed into the PAC. It is used to scale and convert the pneumatic data appropriately before it is fed into the physical components which make up the turbine emulator assembly. In order to gain better insight into the performance exhibited by an OWC device, its pneumatic output must be known for every sea state in which it will likely operate. In a previous set of wave tank experiments conducted at the Hydraulics and Maritime Research Centre [7], a floating OWC scaled prototype was exposed to a multitude of sea states. The prototype was exposed to wave conditions representative of 15 model sea states and the wave tank provided a scale of 1/50 or 0.02 in relation to full scale. These sea states are numbered from B01 to B15 and shown in Fig. 8 as a function of % Occurrence over a year. The full scale wave height and time period in between waves (shown as H and t respectively) relative to every sea state are listed in a table on the right of the figure.

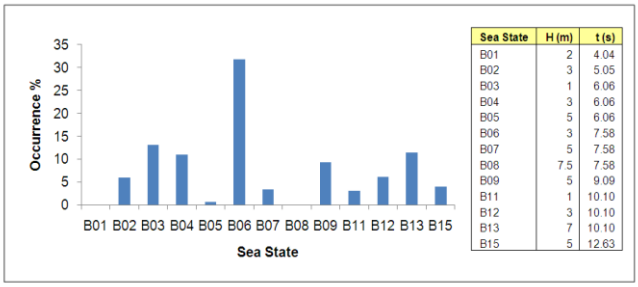

Sea State	H (m)	t (s)
B01	2	4.04
B02	3	5.05
B03	1	6.06
B04	3	6.06
B05	5	6.06
B06	3	7.58
B07	5	7.58
B08	7.5	7.58
B09	5	9.09
B11	1	10.10
B12	3	10.10
B13	7	10.10
B15	5	12.63

Figure 8: Relative occurrence of a given sea state throughout the year

Throughout the experiments, typically lasting 15 minutes per sea state, sensors within the OWC recorded values of air chamber pressure, p, and airflow, Q. Since the pneumatic power, P_{pneu}, provided by the OWC can be expressed by Equation (7),

$$P_{pneu} = pQ \tag{7}$$

the existing data sets could easily be converted to represent pneumatic power versus time. In order to use the pneumatic data in the 20 kW test rig, the values needed to be adjusted appropriately to reflect a scale of 0.36 in relation to full scale [9]. This was accomplished by using the Froude power relation shown in Equation (8).

$$P_{pneu1} = P_{pneu2}\left(\frac{\lambda_2}{\lambda_1}\right)^{3.5} \tag{8}$$

where P_{pneu1}, P_{pneu2} and λ are the scaled pneumatic power for the 20 kW system, the pneumatic power at 1/50th of full scale and the scale factor respectively. The scale factor is equivalent to the inverse of a given scale. Therefore at full scale, $\lambda = 1$, at a scale of 0.02 in relation to full scale, $\lambda = \lambda_2 = 50$, and at a scale of 0.36 in relation to full scale $\lambda = \lambda_1 = 2.79$. The system's mechanical power output, P_{mech}, is equivalent to the product of the pneumatic power input, P_{pneu1}, and the turbine efficiency, η, as shown in Equation (9).

$$P_{mech} = P_{pneu1}\eta \tag{9}$$

The efficiency for a Wells turbine changes considerably depending on the airflow regime. The Wells turbine efficiency curve used in this study [8,9] is shown in Fig. 9 as a function of the flow coefficient, Phi.

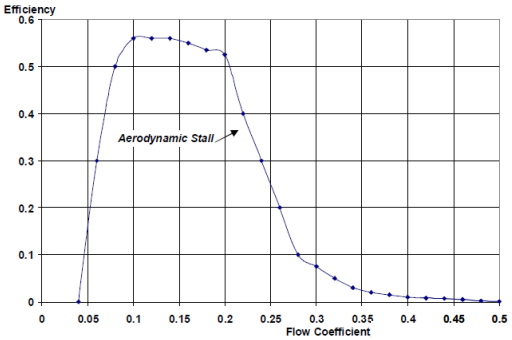

Figure 9: Wells turbine efficiency curve

The flow coefficient is a dimensionless parameter and is defined as the ratio of the airflow velocity, v_a, across the turbine to the tip velocity, U_t, of the turbine blades as demonstrated in Equation (10).

$$\text{Phi} = \frac{v_A}{U_t} = \frac{\left(\frac{Q}{A_D}\right)}{(\omega_t r_t)} = \frac{\left(\frac{Q}{\frac{1}{4}pi \cdot (D_t - D_h)^2}\right)}{\left(\frac{pi \cdot N_t}{30} r_t\right)} \tag{10}$$

where A_D, r_t, D_t, D_h, ω_t and N_t are the turbine duct cross-sectional area, turbine radius, turbine diameter, hub diameter, angular velocity and rotational speed respectively. Airflow values were inputed into Equation (10) for a Wells turbine of known dimensions operating at a known speed and from this it was possible to calculate the equivalent values of the flow coefficient. These flow coefficients were then used to extract the relative turbine efficiencies over time from Fig. 9. Equation (11) could then be derived by substituting Equation (8) into Equation (9).

$$P_{mech} = P_{pneu2}\left(\frac{\lambda_2}{\lambda_1}\right)^{3.5}\eta \qquad (11)$$

The result of solving for P_{mech} in Equation (11) for a given pneumatic data set is a power profile such as is demonstrated in Fig. 10 (in this case for model sea state B06).

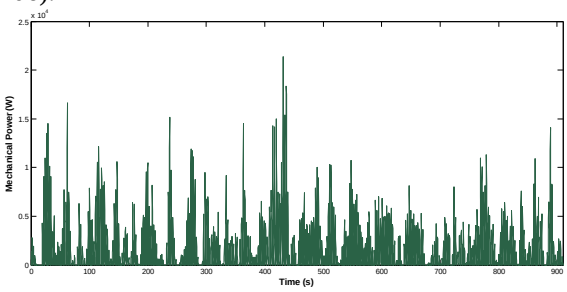

Figure 10: Mechanical power profile for sea state B06

Outputs similar to that which is shown in Fig. 10 make up the virtual component of the turbine emulator and are available for every model sea state. Table 2 summarizes the average and peak mechanical power values achieved for each of the highest occurring sea states.

Table 2: Scaled average & peak mechanical power for model sea states

Sea State	B02	B03	B04	B06	B07	B09	B12	B13	B15
P_{mech_avg} (kW)	1.1	0.16	1.6	1.5	3.3	2.5	0.85	3.2	1.1
P_{mech_peak}(kW)	17	4.1	21	21	21	21	14	21	16
Occurrence	6%	13%	11%	32%	3%	9%	6%	11%	4%

Following Equation (12), P_{mech} is divided by $(pi/30)N_t$, to produce a torque reference signal, M, which can be directly introduced to the motor drive from the PAC.

$$M = \frac{P_{mech}}{\omega_t} = \frac{P_{mech}}{\left(\frac{pi}{30}N_t\right)} \qquad (12)$$

It is important to note that the method used to calculate P_{mech} in this section was for a simplified case in which the turbine efficiency with time was based on a constant shaft speed, N_t, of 1500 RPM. In the current study, variable speed drives are used which enable significant improvements in efficiency depending on the control strategy utilized. This issue will be discussed in greater detail in section 3.4.

3.4 Control Strategy

In this section, a possible control method will be discussed which may be utilized in the wave energy device emulator with the generator working in squirrel cage mode. The generator control is achieved by sending a constant torque signal, M_2, representative of a given sea state to the regenerative drive from the PAC as shown in Fig. 11. The torque will remain constant as long as the conditions which define its related sea state are satisfied. If these conditions are not met, the torque will either increase or decrease to another constant value representative of the new sea state. At any given value of M_2, the shaft speed, N_t, will oscillate about an average value N_{t_avg} ensuring the best aerodynamic performance for the turbine [10]. As N_t is variable, the flywheel will act accordingly to temporarily store energy and soften peaks in the electrical power output. A reading of the instantaneous shaft speed, N_t, will be supplied to the PAC from an encoder located on the induction motor. Based on this feedback, the proper torque signal, M_1, will be generated and fed to the motor drive. This method of calculating the simulated turbine torque differs from that which was discussed in section 3.3 in that N_t now varies with time.

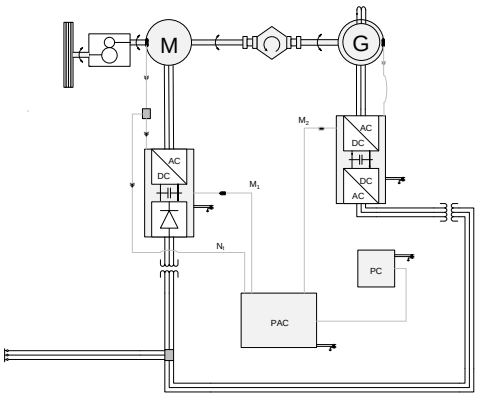

Figure 11: Simplified schematic diagram of test rig with generator working in squirrel cage mode

3.4.1 Generator Control

The flowchart in Fig. 12 shows all the steps which are required to generate the torque signal M_2.

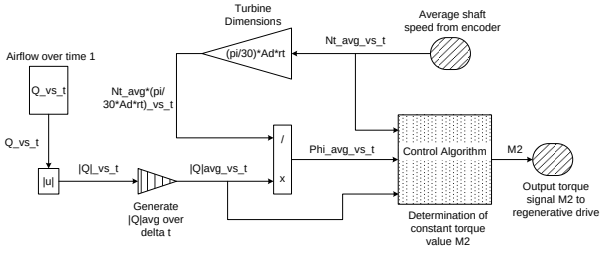

Figure 12: Flowchart indicating steps for calculating M_2

Q_vs_t is the air flow recorded in the OWC with time. An example air flow curve for sea state B06 is shown in Fig. 13. Since the flow is bidirectional, Q

oscillates between positive and negative values. For this reason, the absolute value is taken.

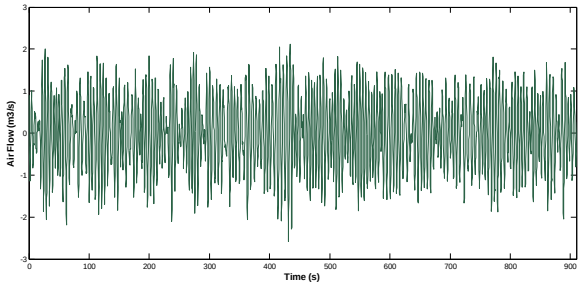

Figure 13: Air flow profile for sea state B06

Average airflow values over time intervals Δt are then calculated in order to provide a profile of average Phi versus time, where Phi is the dimensionless flow coefficient. In doing this, it is necessary to add the average airflow value for the first Δt period to all the time steps which make up the first time interval. This makes up for the time delay which would otherwise occur. To calculate Phi_{avg} , $|Q|_{avg}$ is divided by the product of the turbine duct area, A_D, turbine radius, r_t, shaft speed, N_{t_avg}, (measured in the encoder over the time interval Δt) and a conversion factor of pi/30, as per Equation (10). The next step in the flowchart is the control algorithm which outputs an appropriate value of M_2 based on the Phi_{avg}, Q_{avg} and N_{t_avg} inputs. By referring to Fig. 9, it can be seen that in order to obtain optimum turbine efficiency, the flow coefficient, Phi, must be within a limited range. Equation (10) rewritten below as Equation (13) shows that the average shaft speed has a direct impact on Phi_{avg} for any given value of Q_{avg}. When shaft speed increases, Phi_{avg} decreases and vice versa.

$$\mathrm{Phi_{avg}} = \frac{Q_{avg}}{\left(\frac{pi}{30} A_D r_t N_{t\_avg}\right)} \qquad (13)$$

Therefore, if N_{t_avg} were kept constant during more energetic sea conditions, it is clear that Phi_{avg} would increase simultaneously with Q_{avg}. This would not be desirable since the turbine efficiency would drop as a result. Hence, the generator control must compensate in some way to ensure optimum efficiency. This can be accomplished by assigning constant values of N_{t_avg} and torque, M_2, for different sea states. At any given sea state, the instantaneous shaft speed, N_t, would then be allowed to freely oscillate about this average speed value. The control algorithm in Fig. 12 works as follows: If the boundary conditions shown below are not satisfied, M_2 will be adjusted until Phi_{avg} returns to the optimum point, and the system will then operate at a new N_{t_avg}. The boundary conditions are such that

$$\mathrm{Phi_{avg\_min}} \leq \mathrm{Phi_{avg}} \leq \mathrm{Phi_{avg\_max}}$$
$$\mathrm{N_{t\_avg\_min}} \leq N_{t\_avg} \leq N_{t\_avg\_max}$$

where Phi_{avg_min} and Phi_{avg_max} are the minimum and maximum values intersecting the curve in Fig. 9 at the lowest permissible efficiency and $N_{t\_avg\_min}$ and $N_{t\_avg\_max}$ are the minimum and maximum average shaft speed values tolerated in the system. The average shaft speed limits are constrained by both the practically controllable limits of the drive and/or generator and the underdamping / overdamping limits of the OWC. Too little damping particularly can reduce the pneumatic power availability. As turbine damping is directly proportional to speed, it is clear that limiting the speed range would effectively limit the damping range. If the said boundary conditions are satisfied, the turbine damping will remain within a range as to maximize the output from the OWC at all times and the airflow range will be optimal so as to maximize the turbine's conversion.

3.4.2 Motor Control

In section 3.3, the pneumatic power for a given sea state was converted to mechanical power after the data was scaled appropriately. Mechanical power values were calculated for a single sea state, B06, and the turbine shaft speed was assumed to be constant at 1500 RPM. In order to have better performance over a wide range of sea states and make efficient use of the flywheel, section 3.4 describes a control method which changes the average shaft speed, N_{t_avg}, depending on the sea state and allows N_t to oscillate about its value. This value of N_t would then be fed back to the PAC and used to control the motor. Fig. 14 shows the motor control system and outlines all the steps which are required in order to generate the torque signal M_1. The section on the left of Fig. 14 illustrates a method for calculating Phi which is almost identical to that described in Fig. 12 for calculating Phi_{avg}. The only difference is that instantaneous values of shaft speed are used in the calculation instead of average values.

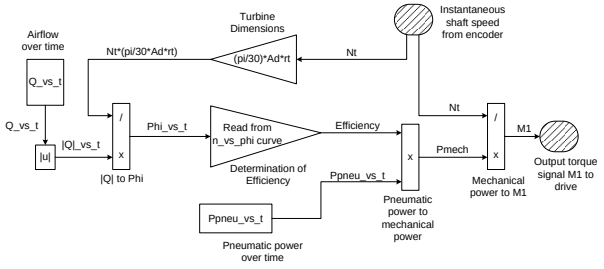

Figure 14: Flowchart indicating steps for calculating M_1

Based on the Phi value, the efficiency can then be determined from the Phi versus efficiency curve, shown in Fig. 9. Once the efficiency is known, its value is multiplied by pneumatic power, P_{pneu} in order to get mechanical power, P_{mech}. An example pneumatic power curve for sea state B06 is shown in Fig.15. Section 3.3 shows the mechanical power curve, Fig. 10, for sea state B06 calculated by assuming a constant N_t value of 1500 RPM. If the mechanical power curve were to be calculated using the variable speed control

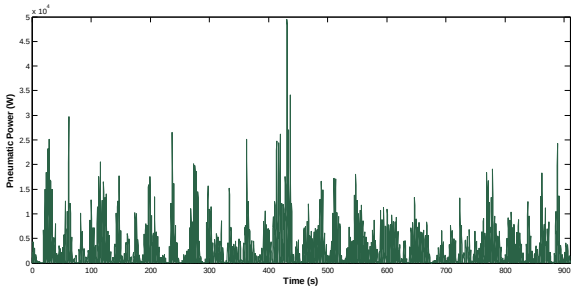

Figure 15: Pneumatic power profile for sea state B06

strategy described in this section, the results would be significantly different. Once P_{mech} is calculated, it is divided by the instantaneous shaft speed, N_t, generating the reference torque signal M_1 as shown by Equation (12).

3.5 Flywheel Energy Storage

It was stated in section 2.4 that energy could be stored or retrieved on demand by controlling the rotational speed of the flywheel. In order to test this theory, a Matlab/Simulink model, shown in Fig. 16, was constructed from Equations (3) & (4) and incorporated into the current study.

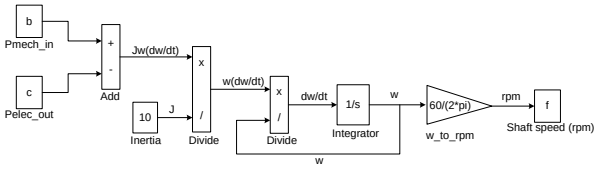

Figure 16: Matlab/Simulink model showing speed variation of the shaft "f" as a result of the mechanical power exerted by the motor "b" and the electrical power produced by the generator "c"

The model is useful in calculating variations in shaft speed when the drives are torque controlled. The system's inertia was inputted into the model and simulations were done using a fixed-step, ode5 solver. The inertia term, J, is equivalent to 10 kgm^2 and was calculated from Equations (14) & (15).

$$J = J_{fw} + J_{dt} \tag{14}$$

$$J_{fw} = \frac{m^2}{2 \cdot pi \cdot \rho \cdot h} \tag{15}$$

where m, ρ and h are the flywheel's mass, density and thickness respectively, as described in section 2.1. The values were subbed into Equation (15) and the flywheel inertia term, J_{fw}, was found to be 8 kgm^2. The drive train inertia, J_{dt}, was then assumed to be approximately 2 kgm^2 and added to J_{fw} in Equation (14) to solve for J. The initial shaft speed was set at 1500 RPM and the power input matrices, shown as "b" and "c" in the Simulink model, were taken from the wave tank test data discussed in section 3.3. Acceptable lower and upper limits for shaft speed were set to 1150 RPM and 1850 RPM respectively for the simulation with an average shaft speed of 1500 RPM. As for the input data, of the 15 Sea states, B06 was chosen as the most suitable case for design since it is the most frequently occurring sea state with the highest power variation with time. Because of this, it could be considered a worst case scenario and therefore a good candidate to test the performance of the flywheel. The input "b" from Fig. 16 represents the mechanical power exerted by the turbine with time under sea state B06 and is identical to the profile shown in Fig. 10. The input "c" from Fig. 16 represents the electrical power produced by the generator and was chosen to be a moving average of "b" with a 30 second delay. In other words, the first 30 seconds of data in the "c" array is equivalent to the average power calculated in the first 30 seconds in the "b" array. The next data point in "c" is then the 30 second average power calculated starting one data point lower in the "b" matrix and so on. This method ensures that the power released to the grid varies within acceptable limits and allows the flywheel to store and release energy as required throughout keeping the shaft speed within the allotted boundaries. The output "f" from Fig. 16 represents the shaft speed variation with time. The power and resultant shaft speed curves are shown in Fig. 17 for sea state B06. The red and blue curves in the upper diagram in Fig. 17 are equivalent to the electrical power output matrix "c" and mechanical power input matrix "b", respectively, in Fig. 16. The lower diagram describes the shaft speed variation with time and is equivalent to matrix "f" in Fig. 16. A convenient method utilized to assess the performance of the flywheel was to compare the peak to average ratio of the electrical power output with and without the flywheel in the system. Table 3 lists the values of peak and average electrical power output for sea states B06 and B13 as well as the resultant ratio of both values.

Table 3: Ratio of peak to average electrical power output for sea states B06 and B13 with and without a flywheel

Sea State	$P_{elec\_out\_peak}$ (kW)	$P_{elec\_out\_avg}$ (kW)	$P_{elec\_out\_peak}$ / $P_{elec\_out\_avg}$
B06 (with flywheel)	4.7	1.5	3.1
B06 (without flywheel)	21	1.5	14
B13 (with flywheel)	7.4	3.2	2.3
B13 (without flywheel)	21	3.2	6.6

A simulation was conducted for sea state B13 as it is of relatively high power and occurrence. Additionally, it provides an extra value for comparison in the performance analysis. Peak and average electrical power output values (without flywheel) were taken from Table 2 since $P_{elec} \approx P_{mech}$ when no energy storage is present in the system. The electrical power output values (with flywheel) were taken from Fig. 17. Table 3 shows that the power ratio for sea state B06 (without flywheel) reduces by a factor of approximately 4.5 from 14.02 to 3.11 with the addition of the flywheel to the system. This implies that significant improvements in performance can be achieved by adding a flywheel. Similarly, for sea state B13, the performance is seen to increase by a factor of nearly 3.

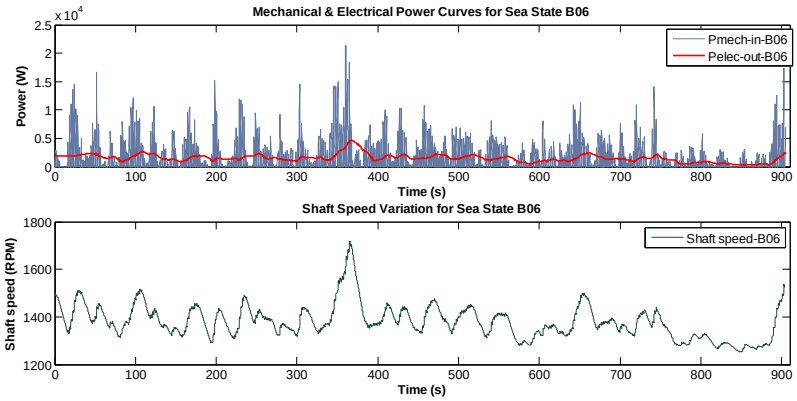

Figure 17: Matlab/Simulink model showing flywheel simulation results for sea state B06

4 Conclusions

Until now, a crucial middle step has been missing in the design and implementation process for wave energy converter (WEC) devices. Scaled WEC devices being tested at ocean sites are commonly designed based on test data recorded from WEC prototypes in laboratory wave tanks. However, little to no information is known beforehand as to which electrical configuration and control system is best suited for a WEC in a given location. This design limitation has been overcome by running system simulations but falls short in the end in that no real hard data can be provided. Constructing a WEC device designed in this way and deploying it on site for testing involves great risk. This is mainly due to the fact that the components are fixed and are not easily interchangeable. Experience has shown that if a problem arises at this later stage of testing, the time and expense required to fix it can be quite considerable.

In the current work, the design of a unique experimental test rig has been presented. Its purpose is to recreate within a laboratory setting the dynamic response of a prime mover onto a motor – generator set and measure the outgoing power quality through a grid emulator. The test rig is extremely flexible in that the prime mover can simulate from real or modelled time series data any varying source, multiple generator configurations are possible, the flywheel inertia is variable and any control algorithm may be implemented. Therefore, real test data may be provided for a scaled model under controlled conditions. The experimental wave energy device emulator test rig essentially provides the missing middle step which is needed to fully optimize a WEC device before it is constructed.

A case study was considered in the present work in which data from an OWC – Wells turbine device operating under a number of sea states was incorporated into the test rig. A control method was proposed for the variable speed squirrel cage generator arrangement which designates a constant torque and an average shaft speed to a given sea state. The method was chosen as it allows instantaneous speed variations about the average shaft speed value, enabling the flywheel to be utilized to its full potential. Simulations were conducted in Matlab/Simulink to test the effectiveness of the flywheel in the wave energy device emulator and results show that system performance improved greatly with its addition. Peak to average ratios for power exported to the grid were seen to improve by up to a factor of 4.5. These preliminary simulation results will be verified experimentally with the test rig and comparisons will be drawn.

5 Acknowledgements

The author would like to thank the management of the Hydraulics & Maritime Research Centre for providing the time and resources necessary for completing this work. The author would also like to thank the SEI Ocean Energy Development Unit for funding this project through the implementation of Energy Minister Eamon Ryan's Ocean Energy Strategy for Ireland.

6 References

[1] E. Block, “Tidal Power: an Update”, Renewable Energy Focus, Nov. 2008, pp. 58-61.

[2] M. Mueller, R. Wallace, “Enabling Science and Technology for Marine Renewable Energy”, Energy Policy, vol. 36, Oct. 2008, pp. 4376-4382.

[3] Dept. of Com., Mar. & Nat. Res., “Ocean Energy in Ireland”, October 2005.

[4] L. Kadar, P. Hacksel, J. Wikston, “The Effect of Current and Voltage Transformers Accuracy on Harmonic Measurements in Electric Arc Furnaces”, IEEE Transactions on Industry Applications, Vol.33, No.3, May/June 1997.

[5] Cape Wind Associates LLC, “115kW Solid Dialectric Submarine Cable”, Technical Specifications, Section 6, January 2004.

[6] R. Alcorn, “Wave Station Modelling Based On The Islay Prototype Plant”, PHD Thesis, Queen’s University of Belfast, 2000.

[7] J.B. Saulnier, “Design of the OWC Buoy”, Project Report, UCC-HMRC, September 2004.

[8] R. Curran, T.J.T. Whittaker and T.P. Stewart, “Aerodynamic Conversion Of Ocean Power From Wave To Wire”, Energy Convers. Mgmt, Vol.39, No. 16-18, 1998, pp.1919-1929.

[9] D.L. O’ Sullivan, A.W. Lewis, “Generator Selection For Offshore OWC Wave Energy Converters”, European Power Electronics Conference, Sept., 2008.

[10] P. A. P. Justino, A. F. De O. Falcao, “Rotational Speed Control of an OWC Wave Power Plant”, Journal of Offshore Mechanics and Arctic Engineering, Vol. 121, May 1999, pp.65-77.